Chalcogenide Letters Vol. 21, No. 12, December 2024, p. 1021 - 1034

Pressure induced structural, anisotropy and thermal characteristics of $MgIn_2S_4$

L. M. Pu [a,*], S. G. Pei [a], X. H. Tang [a], Z. Yin [b], H. J. Hou [b], H. L. Guo [c]
[a] *Yancheng KinderGarten Teachers College, Yancheng, 224051, China*
[b] *School of Materials Science and Engineering, Yancheng Institute of Technology, Yancheng, Jiangsu 224051, China*
[c] *College of Electronic and Information Engineering, Yangtze Normal University, Fuling, 408000, Chongqing, China*

The structural parameter, elastic anisotropy, and thermal properties of cubic $MgIn_2S_4$ under pressures is examined using first principles techniques. The determined lattice constant exhibits a high level of concurrence with the values reported in existing literature. Based on the mechanical characteristics, there is an observed enhancement in both ductility and anisotropy of $MgIn_2S_4$ under increased pressure. The investigation focuses on the thermal characteristics, encompassing the impact of temperature and pressure on key parameters such as Debye temperature, Grüneisen constant et al.

(Received September 21, 2024; Accepted December 16, 2024)

Keywords: $MgIn_2S_4$, First principles, Elastic properties, Thermal properties

1. Introduction

The AB_2S_4 cubic spinels, where A represents Cd, Zn, and Mg; and B represents In, are intriguing substances with numerous practical uses in fields like optoelectronics, solar energy conversion, hydrogen production, and the degradation of organic dyes [1-5]. Extensive research and investigation have been conducted on $MgIn_2S_4$, a member of this specific subgroup of cubic spinels, for a significant period of time. The FP-APW method was employed by Semari et al. to explore the physical properties of spinels $MgIn_2S_4$ and $CdIn_2S_4$ [6]. The investigation of Bouhemadou et al. focused on examining how pressure affects the thermodynamic properties of $MgIn_2S_4$ and $CdIn_2S_4$ compounds [7]. A study conducted by A. K. Kushwaha and colleagues delved into the examination of the vibrational, mechanical, and thermodynamic characteristics exhibited by MIn_2S_4 indium thiospinels (where M represents Cd, Zn, and Mg) [8]. To the extent of our comprehension, previous studies have examined the mechanical and electronic characteristics of $MgIn_2S_4$, as well as explored its optical properties under 0 GPa conditions. However, there has been no investigation into the mechanical and thermal characteristics of $MgIn_2S_4$ at elevated pressures. Now, theoretical approach is employed to calculate and analyze the impact of pressure on the elastic and thermal properties of $MgIn_2S_4$. We anticipate that our findings will offer ample theoretical backing for future research endeavors focusing on the application of $MgIn_2S_4$.

* Corresponding author: pulmyct@163.com
https://doi.org/10.15251/CL.2024.2112.1021

2. Details of computational methods

All computations are conducted utilizing the density functional theory (DFT) with plane-wave pseudopotentials, as implemented in CASTEP code [9-10]. We utilize vanderbilt-type ultrasoft pseudopotentials (USPP) [11] to characterize the interactions between electrons and ions. The Perdew-Burke-Ernzerhof (PBE-GGA) generalized gradient approximation is employed to account for the impact of exchange-correlation interaction[12]. Through the convergence test, the cut-off energy is 600 eV and the *k*-point is 7×7×7.

3. Results and discussion

3.1. Structural model

The Fd-3mz space group is assigned to $MgIn_2S_4$. Fig. 1 illustrates the structural model of $MgIn_2S_4$, that the coordinates of Mg (0, 0, 0), S(0.384, 0.384, 0.384), In(0.625, 0.625, 0.625), respectively. The lattice constant of $MgIn_2S_4$ can be obtained by referring to literature, $a = b = c =$ 10.6878 Å [14], and the bond angle is $\alpha = \beta = \gamma = 90°$. These are taken as the initial data to construct the atom, and it is geometrically optimized, and the geometrically optimized model is obtained, and its elastic, and thermodynamic properties are studied.

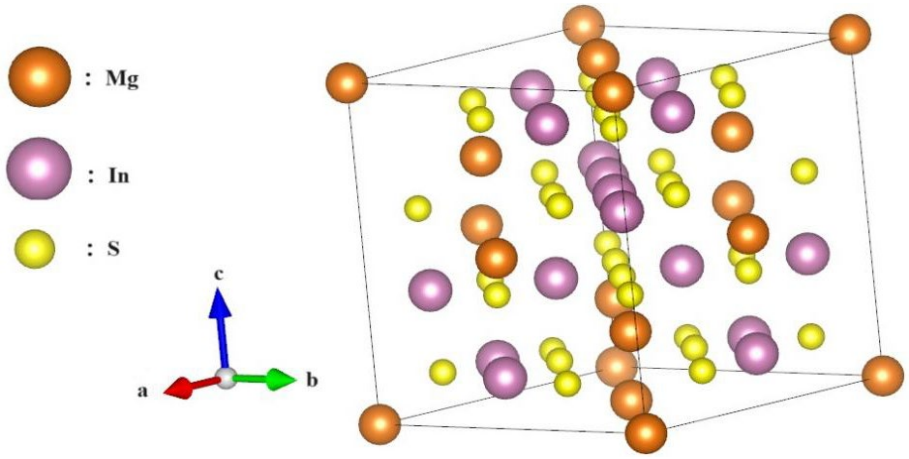

Fig. 1. Crystal structure of cubic $MgIn_2S_4$.

GGA-PBE method was used to determine the optimal design of the structure under the different pressures. The lattice constants of $MgIn_2S_4$, as presented in Table 1, exhibit a strong concurrence with both experimental findings [13, 14] and previously reported theoretical outcomes [6, 7]. Furthermore, the applied pressure leads to a gradual reduction in the lattice constant *a* of $MgIn_2S_4$.

Table 1. The detailed information of lattice constant (a) (Å) of $MgIn_2S_4$ at 0, 2, 4, 6 and 8 GPa, respectively, together with experimental results and the theoretical results.

Pressure (GPa)	0	0		2	4	6	8
$a = b = c$ (Å)	10.8725	10.917[a]	10.6077[b]	10.7805	10.6872	10.6052	10.5302
		10.7108[c]	10.6878[d]				

[a]Cal.[6] [b]Cal.[7] [c]Exp.[13] [d]Exp.[14]

3.2. Anisotropy

The elastic properties directly affect the solid properties of a substance, such as melting point, specific heat and equation of state. $MgIn_2S_4$ is a cubic crystal system consisting of C_{11}, C_{12} and C_{44}. Based on Born's stability criteria, the determination of elastic stability in a pressurized cubic system is as follows[15].

$$(C_{11} + 2C_{12} + P) > 0; (C_{44} - P) > 0; (C_{11} - C_{12} - 2P) > 0 \quad (1)$$

Table 2. The calculated elastic constants C_{ij} (GPa) and S_{ij} (GPa^{-1}) of $MgIn_2S_4$.

Pressure (GPa)	C_{11}	C_{44}	C_{12}	S_{11}	S_{44}	S_{12}
0	81.54	36.38	55.41	0.0272	0.0275	-0.0110
0 cal.[6]	95	38	64			
0 cal.[7]	102.34	26.11	48.62			
0 cal.[8]	119.43	22.37	53.29			
2	89.91	37.33	64.58	0.0278	0.0268	-0.0116
4	97.44	37.94	73.73	0.0295	0.0264	-0.0127
6	103.36	38.10	83.28	0.0344	0.0262	-0.0154
8	109.93	38.51	92.32	0.0390	0.0260	-0.0178

In this analysis, it is evident that the stability conditions are met, indicating the mechanical stability of $MgIn_2S_4$ under these pressures. Table 2 presents our findings for the elastic constants C_{ij} under conditions of zero temperature and pressure, in comparison to values reported in existing literature. The current findings align reasonably well with prior theoretical data [6-8]. When the pressure continues to increase, C_{11} increases successively between 0 and 8 GPa. And with the increase of pressure, C_{12} also increased. However, the sensitivity of C_{44} to pressure is not significantly distinct from that of the other two independent elastic constants.

On this basis, physical elastic parameters (bulk modulus B, shear modulus G, Young's modulus E, Poisson ratio υ) of materials were numerically simulated using Voigt-Reuss-Hill [16-18], and corresponding physical property parameters were obtained and plotted in Fig. 3.

The B and G of a cubic crystal system are expressed the formulas:

$$B_V = B_R = \frac{C_{11} + 2C_{12}}{3} \quad (2)$$

$$B_H = \frac{B_V + B_R}{2} \tag{3}$$

$$G_V = \frac{C_{11} - C_{12} + 3C_{44}}{5} \tag{4}$$

$$G_R = \frac{5(C_{11} - C_{12})C_{44}}{4C_{44} + 3(C_{11} - C_{12})} \tag{5}$$

$$G_H = \frac{G_V + G_R}{2} \tag{6}$$

$$E = \frac{9BG}{3B + G} \tag{7}$$

$$\upsilon = \frac{1}{2}\left(1 - \frac{E}{3B}\right) \tag{8}$$

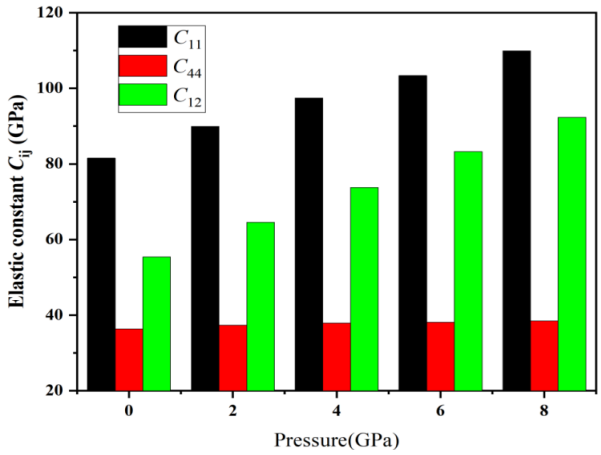

Fig. 2. The change of elastic constants of $MgIn_2S_4$ with pressure.

Pressure positively correlates with the increase of both *B* and *G*, and the change of *E* is relatively small. As depicted in Fig. 3 and documented in Table 3. Under different pressure conditions, the *B* is obviously higher than the *G*, so the shear strength is obviously lower than the compressive strength. *E* is carried to characterize the deformation resistance of solid substances. It is evident from Fig. 3 that the *E* exhibits an initial increase followed by a subsequent decrease as pressure varies. This suggests that the crystal rigidity undergoes enhancement initially with increasing pressure, but eventually diminishes after reaching a peak value.

Table 3. The B, G and E (GPa), Poisson's ratio υ, B/G, Cauchy's pressure ($C_{12} - C_{44}$) (GPa) of $MgIn_2S_4$ at 0, 2, 4, 6, 8 GPa.

Pressure (GPa)	*B*	*G*	*E*	*υ*	*B*/*G*	$C_{12} - C_{44}$
0	64.12	27.05	71.15	0.32	2.37	19.01
0.cal.[6]	66.53	26.40	69.96	0.32	2.52	
0.cal.[7]	74.3	24.0	71.1	0.34	3.10	
0 cal.[8]	75.34	26.17	70.36	0.31	2.88	
2	73.02	27.46	73.21	0.33	2.66	27.25
4	81.63	27.50	74.18	0.35	2.97	35.79
6	89.98	26.88	73.32	0.36	3.35	45.18
8	98.19	26.63	73.26	0.38	3.69	53.81

The determination of material brittleness and ductility can be based on parameters such as *B*/*G*, Poisson's ratio *v*, and Cauchy's pressure (C_{12} - C_{44})[19-21]. Based on Fig. 3 and Table 3, we found that $MgIn_2S_4$ is a ductile material. The ductility exhibits a positive correlation with the rise in pressure.

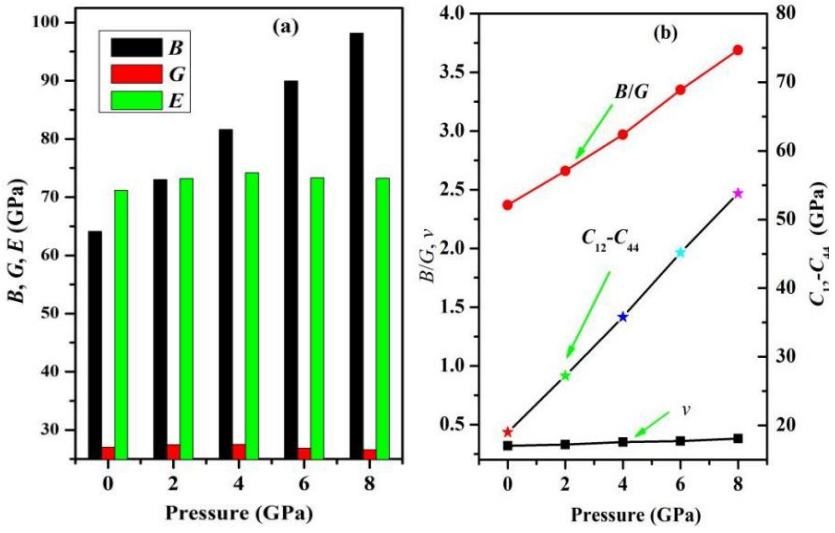

Fig. 3. The change of B(GPa), G(GPa), E(GPa), B/G, v and C_{12}-C_{44} of $MgIn_2S_4$ with pressure.

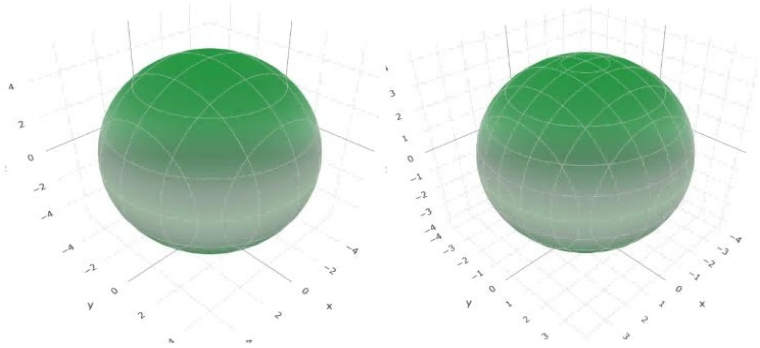

(0 GPa) (4 GPa)

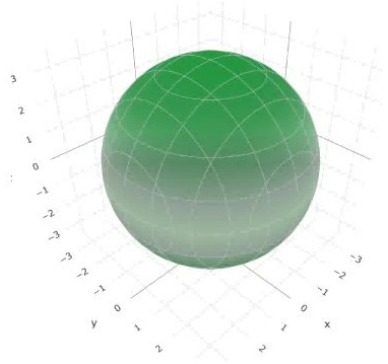

(8GPa)

Fig. 4 The spatial representation of β (TPa^{-1}) of $MgIn_2S_4$.

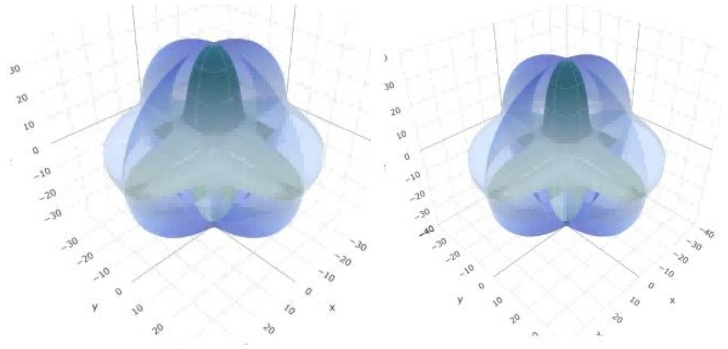

(0 GPa) (4 GPa)

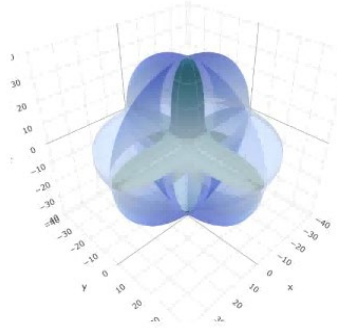

(8GPa)

Fig. 5 The spatial representation of G (GPa) of $MgIn_2S_4$.

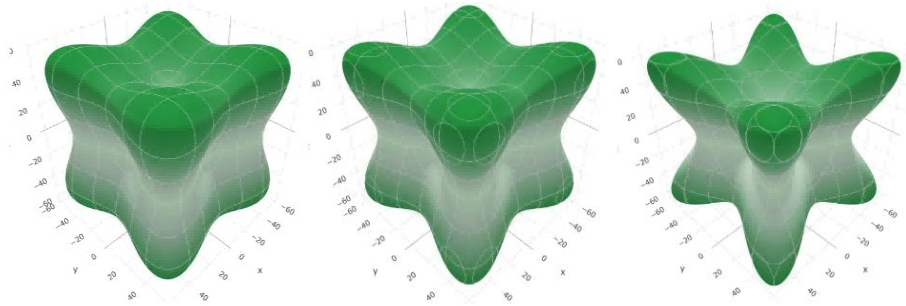

(0 GPa) (4 GPa) (8GPa)

Fig. 6 The spatial representation of E (GPa)of $MgIn_2S_4$.

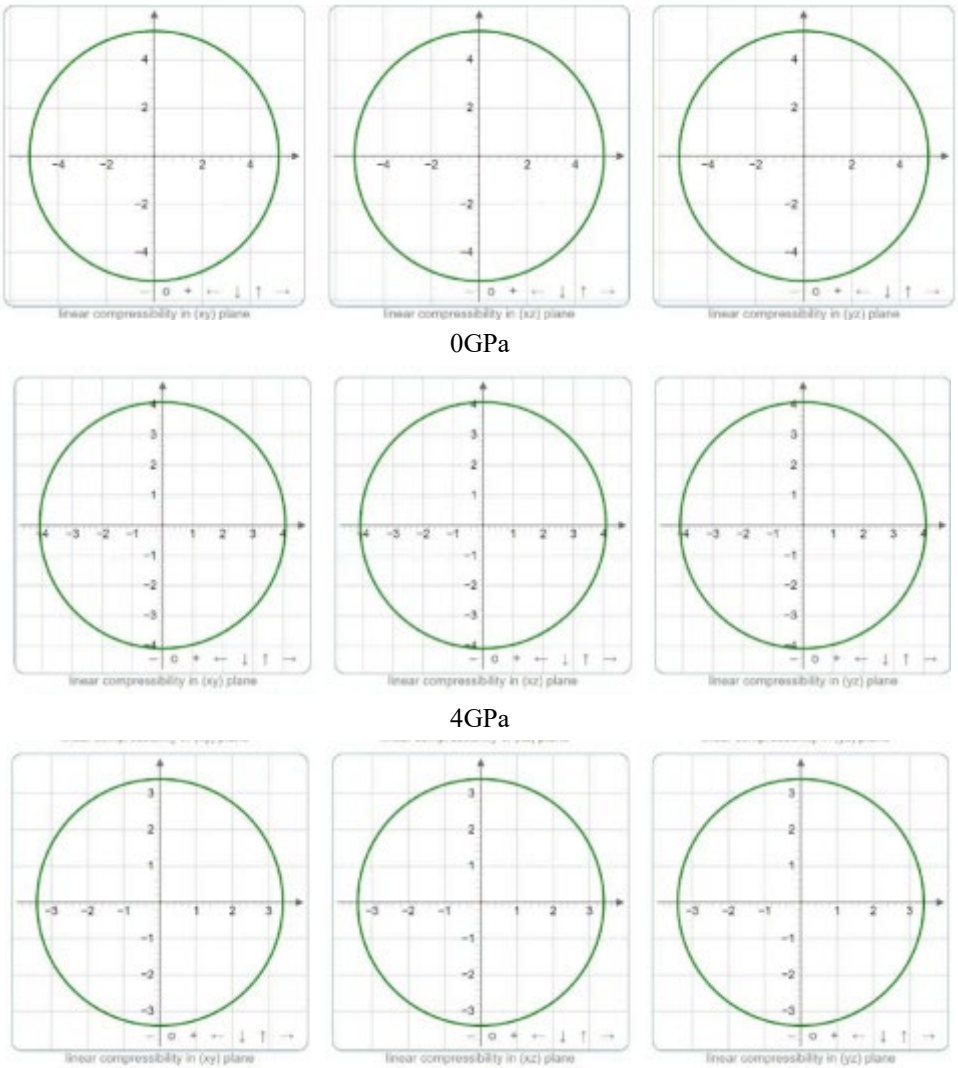

0GPa

4GPa

8GPa

Fig. 7. Estimations of β (TPa^{-1}) in different planes of $MgIn_2S_4$.

In an effort to comprehend the anisotropic characteristics of $MgIn_2S_4$, we have developed three-dimensional (3D) and two-dimensional (2D) plane projections that incorporate linear compressibility β, G, and E [22-23]. In Fig. 4, under different pressures, all 3D surfaces do not deviate significantly from the sphere. Furthermore, it is evident from the data presented in Fig. 5-6 that the G and E values of all 3D structures exhibit substantial deviation from a spherical shape under varying pressures. This observation provides further evidence to support the notion that $MgIn_2S_4$ displays pronounced anisotropic characteristics. The systematic characterization of β, G, and E at various pressures did not yield conclusive results regarding their 3D surface structure. Therefore, the anisotropy of the 3D system of $MgIn_2S_4$ can be systematically studied by 2D planar projection. Fig.7-9 plot 2D plane projections of β, G, E on the different planes under varying levels of pressure, more intuitively describing the elastic anisotropy of $MgIn_2S_4$. Under 0, 4, 8 GPa, the projection of the material on the different all deviates from the circle, indicating that the material has anisotropy on the different planes. From Fig. 8-9, it is found that the projection of $MgIn_2S_4$ deviates from the circle, indicating that $MgIn_2S_4$ has strong anisotropy.

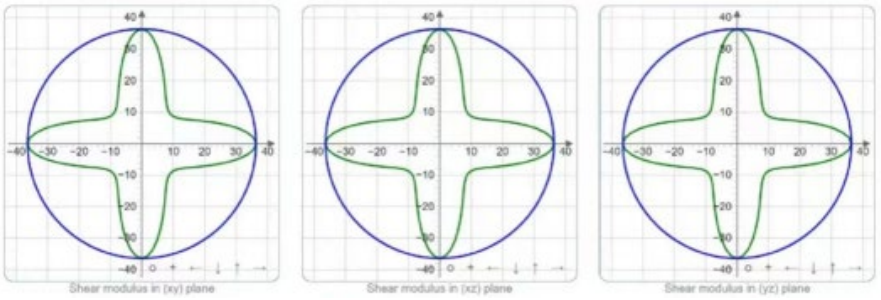

0GPa

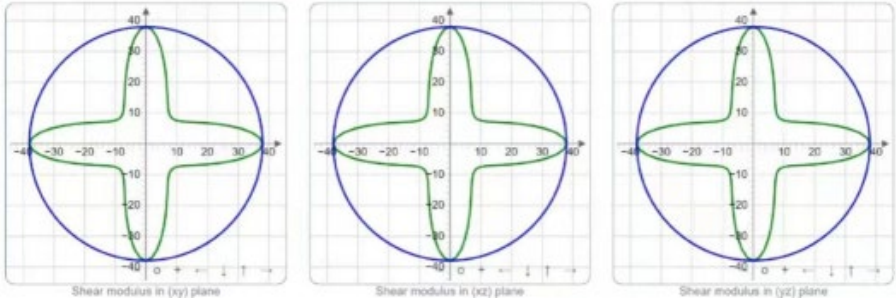

4GPa

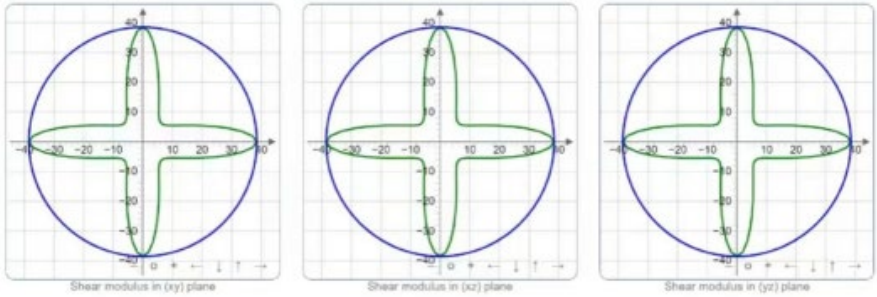

8GPa

Fig. 8. Estimations of G(GPa) in different planes of $MgIn_2S_4$.

Table 4. The range of β (TPa^{-1}) and G (GPa), as well as E (GPa), for $MgIn_2S_4$ under different pressures: 0, 2, 4, 6, and 8 GPa.

Pressure(GPa)	β_{max}	β_{min}	G_{max}	G_{min}	E_{max}	E_{min}
0	5.1984	5.1984	36.379	13.063	91.773	36.698
2	4.5647	4.5647	37.326	12.665	95.675	35.918
4	4.0832	4.0832	37.936	11.854	98.543	33.921
6	3.7047	3.7047	38.096	10.039	100.15	29.038
8	3.3948	3.3948	38.513	8.8021	102.18	25.640

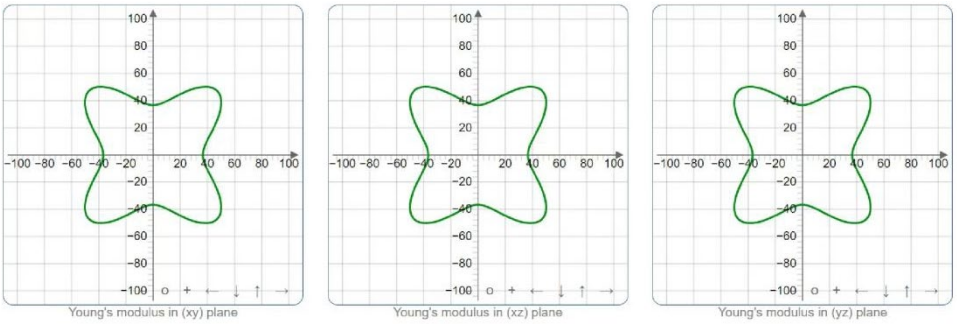

0GPa

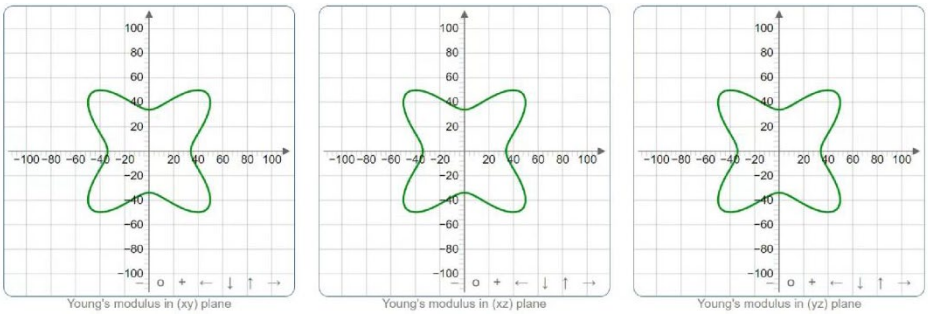

4GPa

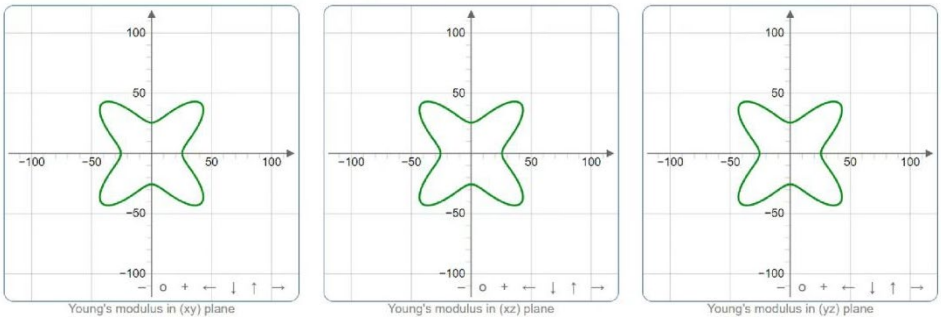

8GPa

Fig. 9. Estimations of E (GPa) in the different planes for $MgIn_2S_4$.

Table 4 lists in detail the parameters of $MgIn_2S_4$ under different pressures, including its maximum and minimum linear compressibility (β_{max}, β_{min}), shear modulus (G_{max}, G_{min}), Young's modulus (E_{max}, E_{min}). In addition, by calculating G_{max}/G_{min} and E_{max}/E_{min}, we further analyze the elastic anisotropy of $MgIn_2S_4$ subjected to varying levels of pressure. Specifically, under pressure conditions of 0 GPa, 2 GPa, 4 GPa, 6 GPa and 8GPa, the G_{max}/G_{min} values of $MgIn_2S_4$ are 2.785, 2.947, 3.200, 3.795 and 4.375, respectively. The corresponding E_{max}/E_{min} values are 2.501, 2.664, 2.905, 3.449, and 3.985, respectively. These values clearly reflect the changing trend of elastic properties of $MgIn_2S_4$. In conclusion, the anisotropy of G, E of $MgIn_2S_4$ showed an increasing trend as the pressure rises.

3.3. Thermal characteristics

To determine the thermal characteristics of $MgIn_2S_4$, we employ the quasi-harmonic Debye model[24]. Fig. 10 depicts the outcomes achieved through the utilization of a particular combination of crystallization parameters, showcasing the determination of both total energy E and volume V.

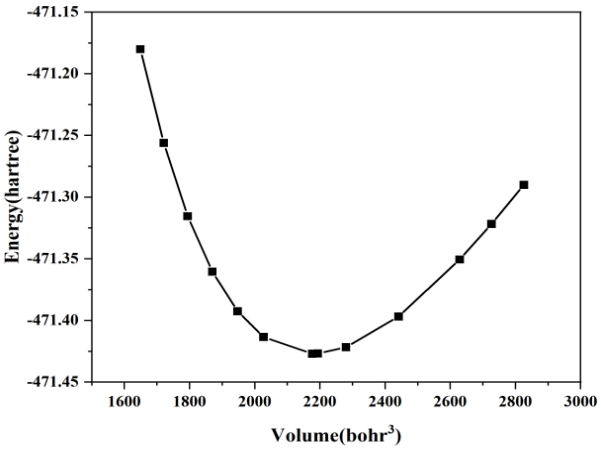

Fig. 10. The total energy E change with volume V for $MgIn_2S_4$.

The Fig. 11 illustrates the B change with temperature T at 0 GPa. At $T < 100$ K, the value of B is large and remains essentially unchanged. Above 100 K, the temperature increases, and the value of B gradually decreases. From this, $T < 100$ K, the lattice constant a of the $MgIn_2S_4$ remains basically unchanged, while the volume V of the cell also remains basically unchanged. If the temperature exceeds 100 K, the temperature will increase, the lattice constant will increase, and the volume V of the cell will increase, so B will gradually decrease. The fourth order polynomial of B with respect to T is obtained by linear fitting:

$$B=67.59-0.00212T-2.39796\times10^{-5}T^2+2.86402\times10^{-8}T^3-1.20629\times10^{-12}T^4 \quad (9)$$

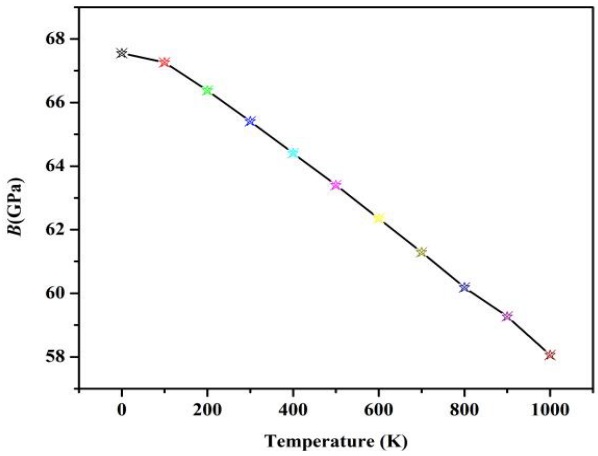

Fig. 11. The B change with temperature T at 0 GPa.

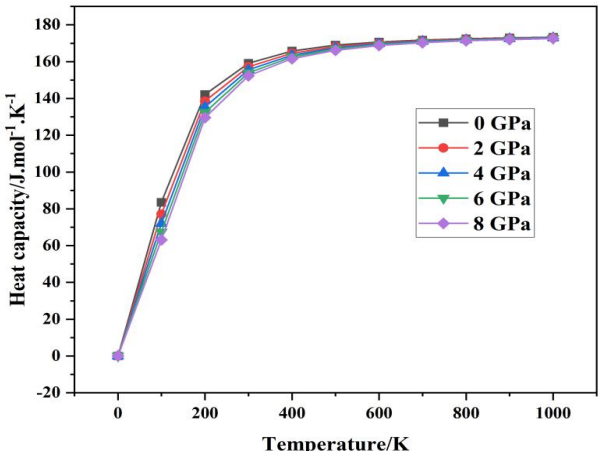

Fig. 12. The C_V change with temperature at 0, 2, 4, 6 and 8 GPa.

In Fig.12 that the heat capacity C_V exhibits an exponential growth with temperature for T < 300 K. However, at higher temperatures, its value approaches the Dulong-Petit limit.

Table 5. The calculated S ($J.mol^{-1}\cdot K^{-1}$), Θ (K), γ of the $MgIn_2S_4$ at T (100, 400, 700, 1000) (K) and P (0, 2, 4, 6, 8)(GPa).

T/K	*P*/GPa	0	2	4	6	8
100	*S*	42.022	37.126	33.510	30.433	27.795
	Θ	416.75	442.94	464.96	485.96	506.02
	γ	2.160	2.071	2.004	1.946	1.894
400	*S*	232.938	222.523	214.069	206.610	199.932
	Θ	410.14	436.83	459.93	481.45	501.70
	γ	2.185	2.091	2.019	1.958	1.905
700	*S*	331.024	319.719	309.522	302.232	295.046
	Θ	402.13	429.52	455.88	475.76	496.25
	γ	2.216	2.115	2.031	1.973	1.919
1000	*S*	396.121	384.235	373.677	365.671	358.176
	Θ	393.98	421.97	448.53	469.80	490.65
	γ	2.250	2.141	2.053	1.990	1.933

In Table 5, we obtained the *S*, *Θ* and *γ* at different temperatures (100, 400, 700 and 1000 K) and different pressures (0, 2, 4, 6 and 8 GPa). Under constant pressure, entropy *S* and Grüneisen constant *γ*, there is a noticeable rise in the trend as the temperature increases. On the contrary, when the temperature remains unchanged, the entropy *S* decreases gradually as the pressure increases, while Debye temperature *Θ* gradually increases, and Grüneisen constant *γ* also shows a downward trend. Specifically, as the pressure gradually rises from 0 GPa to 8 GPa, it is observed that under different temperature, the entropy *S* decreases by 0 %, 24.80 %, 17.18 %, 14.55 %, 13.21 % and 12.44 %. Debye temperature increased by 35.00 %, 35.45 %, 36.55 %, 37.74%, 38.98% and 40.33 %. The decrease of Grüneisen constant *γ* is 16.61%, 16.85%, 17.45%, 18.11%, 18.74% and 19.51%, respectively. Furthermore, it has been observed that as the pressure rises, entropy *S* decreases more significantly at lower temperature than at higher temperature. The Debye temperature exhibits a greater rate of increase at elevated temperatures as opposed to lower temperatures. Regarding the Grüneisen constant γ, its rate of decrease is more pronounced at elevated temperatures compared to lower temperatures. In addition, we obtained *Θ* = 417 K, which agrees excellently with the result 391, 378 and 362 K of Ref. [6-8]. It suggests that the thermal calculations conducted for $MgIn_2S_4$ can be considered trustworthy.

4. Conclusions

We have conducted an analysis on the structural parameter, anisotropy, and thermal characteristics of $MgIn_2S_4$ in our study. The determined lattice constant and elastic constants demonstrate concurrence with the currently available experimental or theoretical data regarding their structural characteristics. The mechanical stability of $MgIn_2S_4$ is confirmed as its elastic constants satisfy the Born criteria.

The anisotropy of G and E in $MgIn_2S_4$ exhibited a rising tendency as the pressure increased. We have provided data on the Θ, as well as the C_V, with respect to variations in temperature T and pressure P. These findings hold significant value in facilitating crystal growth.

References

[1] S. Yang, L. Li, W.H. Yuan, Z.L. Xia, Dalton T. 44, 6374 (2015); https://doi.org/10.1039/C5DT00147A

[2] I. Aguilera, P. Palacios, K. Sánchez, P. Wahnón, Phys. Rev. B 81, 075206 (2010)

[3] S.N. Baek, T.S. Jeong, C.J. Youn, K.J. Hong, J.S. Park, D.C. Shin, Y.T. Yoo, J. Cryst. Growth 262, 259 (2004); https://doi.org/10.1016/j.jcrysgro.2003.10.019

[4] C. Zeng, Q. Zeng, C. H.Dai, L. K. Zhang, Y. M. Hu, Appl. Surf. Sci. 542, 148686 (2021); https://doi.org/10.1016/j.apsusc.2020.148686

[5] C. Tablero, J. App. Phys. 114, 033713 (2013); https://doi.org/10.1063/1.4816102

[6] F. Semari, R. Khenata , M. Rabah, A. Bouhemadou, S. Bin Omran, Ali H. Reshak, D. Rached J., Solid State Chem., 183, 2818 (2010); https://doi.org/10.1016/j.jssc.2010.09.022

[7] A. Bouhemadou, K. Haddadi, R. Khenata, D. Rached, S. Bin-Omran, Physica B 407, 2295 (2012); https://doi.org/10.1016/j.physb.2012.03.017

[8] A. K. Kushwaha, R. Khenata, S. Bin Omran Int. J. Mod. Phys. B, 30, 1650018 (2016); https://doi.org/10.1142/S0217979216500181

[9] P. Hohenberg, W. Kohn Phys. Rev. B 136, 864 (1964); https://doi.org/10.1103/PhysRev.136.B864

[10] W. Kohn, L. J. Sham Phys. Rev. A 140, 1133(1965); https://doi.org/10.1103/PhysRev.140.A1133

[11] D. Vanderbilt, Phys. Rev. B 41, 7892 (1990); https://doi.org/10.1103/PhysRevB.41.7892

[12] J.P. Perdew, K. Burke, M. Ernzerhof , Phys. Rev. Lett.77, 3865 (1996); https://doi.org/10.1103/PhysRevLett.77.3865

[13] M.J. Mehl, B.M. Klein, D.A. Papaconstantopoulos, Intermetallic Compounds: Principles and Practice, Vol. I: Principles, John Wiley and Sons, London, 1995.

[14] H. Hahn, W. Klingler, Z. Anorg. Allg. Chem. 263, 177 (1950); https://doi.org/10.1002/zaac.19502630406

[15] M. Born, K. Huang, Dynamical Theory of Crystal Lattices (Oxford: Clarendon) 1954.

[16] W. Voigt Lehrbuchder Kristallphysik Teubner Leipzig (1928)

[17] A. Reuss, Z. Angew. Math. Mech. 9, 49 (1929); https://doi.org/10.1002/zamm.19290090104

[18] R. Hill, Proc. Phys. Soc. 65, 349 (1952); https://doi.org/10.1088/0370-1298/65/5/307

[19] S. F. Pugh, Philos. Mag. 45, 823 (1954); https://doi.org/10.1080/14786440808520496

[20] D.G. Pettifor, Mater. Sci. Technol. 8, 345 (1992); https://doi.org/10.1179/026708392790170801

[21] N.L. Xu, Y. Chen, S.J. Chen, S. Li, W.B. Zhang, Int. J. Hydrogen Energy 50, 114 (2023); https://doi.org/10.1016/j.ijhydene.2023.06.254

[22] R. Gaillac, P. Pullumbi, F.-X. Coudert, J. Phys. Condens. Matter 28, 275201 (2016); https://doi.org/10.1088/0953-8984/28/27/275201

[23] H. J. Hou, F. Su , H. Y. Wang, W. X. Chen, X. W. Lu, S. R. Zhang, L. H. Xie Chalcogenide Lett. 21, 189 (2024)

[24] M. A. Blanco, A. Martín Pendás, E. Francisco, J. M. Recio, R.Franco, J. Mol. Struc-Theochem. 368, 245(1996); https://doi.org/10.1016/S0166-1280(96)04658-1